

Andre Marziali¹
Joel Pel¹
Dan Bizzotto²
Lorne A. Whitehead¹

¹Department of Physics
and Astronomy

²Chemistry Department,
University of British Columbia,
Vancouver, BC, Canada

Novel electrophoresis mechanism based on synchronous alternating drag perturbation

We present a novel means of transporting molecules in solution by applying a zero-time-average alternating motive force to the molecules, and perturbing the molecular drag coefficient synchronously with the applied force, thus causing a net drift in a direction determined by the phase of the alternating drag perturbation relative to the alternating force. We apply an electrophoretic form of the method to transport and concentrate DNA in a gel, such that all molecules migrate on average away from the nearest electrode and toward a central region. Since an electrode does not occupy this central region, this method presents the possibility of transporting and focusing DNA and other charged molecules in regions free from electrodes and the associated electrochemistry.

Keywords: DNA / Drag alteration / Focusing / Mobility / Multidimensional electrophoresis

DOI 10.1002/elps.200406140

1 Introduction

1.1 General aspects

Electrophoretic particle transport is typically performed in one dimension by applying a direct current (DC) electric field and is therefore limited to transport of particles toward one of the electrodes. Though this is desirable in most applications, in some it would be beneficial to have a more versatile form of electrophoretic transport. For example, it may be advantageous to transport and concentrate particles in a region that is free of electrodes to avoid electrochemical interactions between the electrodes and the particles. Concentration and purification of nucleic acids is one such case – electrochemistry of DNA at the electrophoresis electrodes results in DNA damage [1, 2] and complicates the use of electrophoresis for concentration applications. Laborious and/or expensive purification methods [3–5] must often be employed to prepare nucleic acid samples for many biochemical assays. Though interaction of DNA with electrodes has been circumvented in some applications [6], it remains desirable to devise a completely electrophoretic method for concentration and manipulation of charged polymers in a uniform medium, such that molecules can be transported and concentrated in regions free of electrodes. Such a method could be an inexpensive alternative to poly-

merase chain reaction (PCR) for creating large concentrations of DNA. This is particularly true for large volumes where PCR becomes prohibitively expensive. Detailed discussion of possible applications is beyond the scope of this manuscript, which presents the basic concept of charged molecule transport and concentration by synchronous mobility or drag perturbation.

Alternate forms of electrophoresis (reviewed in [7]) employing time varying or spatially varying fields have already been used to separate and manipulate charged polymers including DNA. For example, it has been shown that an asymmetric alternating current (AC) waveform can cause net drift of electrophoretic particles due to non-linearity of the dependence of speed on electric field [7–14] and that this effect can be used to focus particles in one dimension [15–17]. Dielectrophoresis [18] has been demonstrated capable of concentrating DNA in two or more dimensions [19, 20], but requires high electric field gradients to generate a significant effect.

In this paper, we propose a novel, general principle for achieving multidimensional electrophoresis in alternating electric fields, based on temporal alteration of the coefficient of drag in synchronization with the AC field. For brevity, we will use the acronym SCODA (synchronous coefficient of drag alteration) for this principle. We note that such an approach can concentrate and transport charged particles in one, two, or three dimensions, eliminate electrochemistry problems at electrodes, and may enable new separation techniques. We illustrate the theoretical basis for this effect, discuss possible implementations, and demonstrate it with one specific method involving a combination of rotating and oscillating electric fields to concentrate DNA in solution.

Correspondence: Andre Marziali, Rm 415, Department of Physics and Astronomy, UBC, 6224 Agricultural Rd., Vancouver, BC, Canada, V6T-1Z1

E-mail: andre@physics.ubc.ca

Fax: +604-822-5324

Abbreviations: DC, direct current; SCODA, synchronous coefficient of drag alteration

1.2 The SCODA principle

Consider an electrophoretic particle that has an electrophoretic mobility, μ in an electric field $E = \hat{E}E_0 \cos(\omega t)$. By definition, the particle will move with a velocity given by:

$$\bar{v}(t) = \mu \cos(\omega t) \hat{E}E_0 \quad (1)$$

The time average of $\bar{v}(t)$ is 0.

Suppose, however, that μ is not constant; it is a function of time. If the Fourier transform of μ has a component proportional to $\cos(\omega t)$ the time average of the $\bar{v}(t)$ need not be zero. As a simple example, consider the following time dependency:

$$\mu(t) = \mu_0 + \mu_1 \cos(\omega t) \quad (2)$$

Substituting Eq. (2) in (1), and computing the time average, \bar{v} , we obtain:

$$\bar{v} = \frac{1}{2} \mu_1 \hat{E}E_0 \quad (3)$$

Thus, it is possible to have a non-zero time average velocity, in other words, a net electrophoretic drift, even if the time average of the applied electric field is zero. To achieve this, the effective electrophoretic mobility must have a time dependence that contains an oscillatory component that is synchronized with the field oscillations. There are potentially many ways to achieve such a time dependence of the effective electrophoretic mobility.

One approach is to apply sinusoidal temperature fluctuations, which modulate a solution's viscosity and hence the electrophoretic mobility of its constituent ions. This has been demonstrated (data not shown) to lead to the time-averaged drift velocity described in Eq. (3). This effect can equivalently be interpreted as arising from the temperature dependence of the solution's conductivity.

Optically induced changes in the electrophoretic mobility of a molecule may also be possible; this would enable a very useful form of SCODA. Certain classes of compounds, such as azo-benzene or spiro-pyrans, undergo light induced reversible conformational changes [21]. Azo-benzene can isomerize from the *trans*- to *cis*-form upon exposure to UV light (300 – 400 nm). The conversion back to the *trans*-form occurs once exposed to light with a wavelength greater than 400 nm. This photoisomerization process has recently been used in the creation and dissociation of DNA triplex [22]. Exposure of the 'closed' form of spiro-pyrans to UV light induces isomerization producing an 'open' colored merocyanine species. Reverting to the 'closed' form can be accomplished simply through exposure to visible radiation. The transition between these two forms is accompanied by changes in the polar nature of the molecule. This effect has recently

been used to photochemically manipulate the wetting characteristics of a surface modified with spiro-pyran [23]. These two examples introduce the possibility of optically inducing small but reversible changes in the hydrodynamic drag of a molecule. The electrophoretic mobility of such a molecule, or of a compound containing this molecule, could then be altered in a periodic manner by means of optical excitation. In this case, ω in Eq. (2) is the frequency with which the optical excitation is switched between the wavelength required for the isomerization to one state and the wavelength required for the reverse process. Patterning of the optical excitation over a solution using masks could lead to high resolution concentration of molecules without the need to pattern electrodes or dielectrics in the solution itself as would be required for dielectrophoretic concentration. Though this could be of great use, the challenge in this SCODA implementation remains the development of an appropriate compound that exhibits a sufficient mobility change associated with different conformations, and that can transition rapidly between conformations.

Perhaps the simplest useful implementation of SCODA is purely electrophoretic. By exploiting the small variation of charged polymer mobility with increasing electric field, the SCODA approach allows polymers such as DNA to be concentrated in a uniform homogeneous medium. This is relatively simple, inexpensive, and of potential utility to various biochemical purification processes. This form of SCODA is the principal subject of this paper and its presentation follows in detail.

1.3 Electrophoretic SCODA

Let us consider the case where the speed of a particle is not directly proportional to the electric field. In numerical models (see Section 2 and Fig. 1), we have shown that virtually any nonlinearity can be employed, but it will be helpful in the following explanation to consider a simple example that is amenable to analytic treatment. Let us, therefore, consider the mathematically simple functional relationship in which the particle's velocity is parallel to the field direction and its speed is proportional to the square of the magnitude of the electric field:

$$\bar{v} = k \hat{E}(E)^2 \quad (4)$$

What we would now like to consider is the effective mobility of the particle, in other words the relationship between changes in drift velocity, $d\bar{v}$, and small changes in the electric field $d\vec{E}$.

Expressing $d\bar{v}$ in Cartesian coordinates, we note that in general,

$$dv_x = \frac{\partial v_x}{\partial E_x} dE_x + \frac{\partial v_x}{\partial E_y} dE_y \quad (5)$$

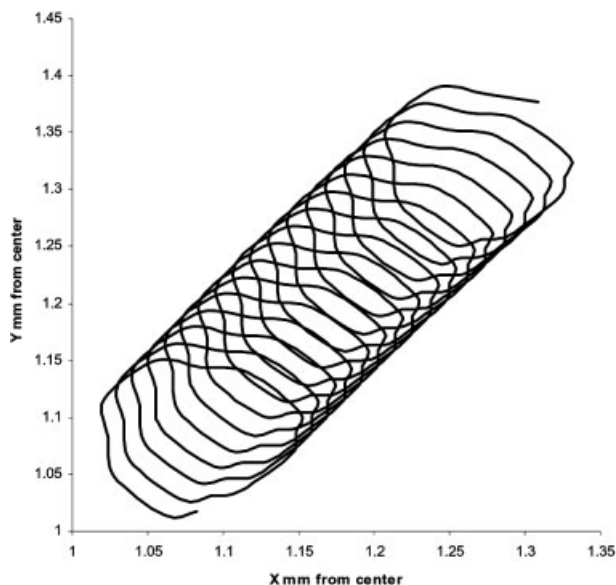


Figure 1. Numerical simulation of particle motion with uniform field rotating at angular frequency ω and quadrupole field oscillating at 2ω . Motion begins at the top right of the path and ends to the bottom left, over 200 s in real time. The rotating fields have been approximated by 12 sequential configurations of potentials as described in Section 2. Each configuration is applied for 1 s. One loop in the particle spiral path corresponds to a full cycle through all 12 potential configurations. The uniform field amplitude is $E = 3845$ V/m at the center of the electrode pattern, the quadrupole field amplitude in the same location is $E_q = 4.2 \times 10^5$ rV/m², or approximately 4200 V/m at 1 mm from the center of the pattern.

$$dv_y = \frac{\partial v_y}{\partial E_x} dE_x + \frac{\partial v_y}{\partial E_y} dE_y \quad (6)$$

Using Eq. (4) to evaluate Eqs. (5) and (6), we obtain a result that is fairly simple:

$$dv_x = k \left[\left(E + \frac{E_x^2}{E} \right) dE_x + \left(\frac{E_x E_y}{E} \right) dE_y \right] \quad (7)$$

$$dv_y = k \left[\left(\frac{E_x E_y}{E} \right) dE_x + \left(E + \frac{E_y^2}{E} \right) dE_y \right] \quad (8)$$

To help interpret this, consider the case where $E_y = 0$ such that $E_x = E$. In this case Eqs.(7) and (8) become:

$$dv_x = 2kEdE_x \quad (9)$$

$$dv_y = kEdE_y \quad (10)$$

This can be interpreted in the following way: the influence of perturbations to the electric field on the particle velocity has a magnitude proportional to that of the ambient field, and if the perturbations are in the same direction as the ambient value of the electric field, they have twice the influence on the velocity than is the case if the perturbation is perpendicular. In other words, an applied electric

field has a direct influence on the effective mobility, that is the ratio of change in velocity to change in field. This means that alternating fields can cause a periodic change in effective mobility. Let us now consider an example of applying this effect to a real electrophoresis problem.

1.4 Creation of a focusing field geometry

Consider a plane in which there is a uniform applied field that rotates counter-clockwise at angular frequency ω , such that the field components are:

$$E_x = E \cos(\omega t) \quad (11)$$

$$E_y = E \sin(\omega t) \quad (12)$$

Now, if we substitute Eq. (11) and (12) in Eq. (7) and (8), and simplify with the aid of trigonometric identities, we will obtain a result which is a sum of constant terms, sine and cosine terms at angular frequency 2ω , and sine and cosine terms at angular frequency 2ω . The subsequent calculations will be carried out in such a way that only the cosine terms at angular frequency 2ω will yield non-zero net drift velocity – therefore we need only evaluate these “ $\cos 2\omega$ ” terms, which we will abbreviate $dv_{x \cos 2\omega}$ and $dv_{y \cos 2\omega}$. We find that:

$$dv_{x \cos 2\omega} = \frac{kE}{2} [\cos(2\omega t)] dE_x \quad (13)$$

$$dv_{y \cos 2\omega} = -\frac{kE}{2} [\cos(2\omega t)] dE_y \quad (14)$$

Now, we can design dE_x and dE_y to take the form of a small quadrupole field that varies in a sinusoidal manner, in proportion to $\cos(2\omega t)$ and intensity coefficient dE_q :

$$dE_x = -dE_q x \cos(2\omega t) \quad (15)$$

$$dE_y = dE_q y \cos(2\omega t) \quad (16)$$

Substituting Eqs. (15) and (16) into Eqs. (13) and (14) and taking the time average, we obtain:

$$\overline{dv_x} = \overline{dv_{x \cos 2\omega}} = -\frac{kEdE_q}{4} x \quad (17)$$

$$\overline{dv_y} = \overline{dv_{y \cos 2\omega}} = -\frac{kEdE_q}{4} y \quad (18)$$

Equations (17) and (18) can be summarized in vector notation:

$$\overline{d\vec{v}} = -\frac{kEdE_q}{4} \vec{r} \quad (19)$$

This shows that for all positions \vec{r} the time averaged drift velocity is in the direction toward the origin, with speed proportional to the mobility coefficient k , the strength of the rotating field E and the strength of the perturbing quadrupole field dE_q . This is an important result since

similar concentration characteristics are not possible with DC fields, as it would require an electric field with negative divergence, in violation of the Maxwell equations.

The treatment above is restricted to motion in a plane, but a similar technique could be applied to achieve concentration in 3-D. This could be achieved by either performing 2-D SCODA sequentially on three orthogonal planes, or by using electrodes lying substantially in a common plane to create the in-plane focusing effect described above, and applying DC voltages on electrodes above and below the center of the plane to direct molecules that lie outside the plane back toward it. Such a DC field would cause a defocusing effect with respect to movement within the plane, but this could be designed to be weaker than the SCODA focusing effect, such that the net result would be focusing in all three dimensions.

It should be noted that while the above calculation used a small perturbing quadrupole field, in order to allow a differential calculation that can easily be solved analytically, there is in reality no restriction that the quadrupole be comparatively small. This is demonstrated in Fig. 1 which shows a numerical simulation (see Section 2) of the particle path for a system in which the magnitude of the rotating fields and quadrupole fields are comparable; similar paths are taken by the particle regardless of its azimuthal starting angle with respect to the center of the electrode system.

2 Materials and methods

2.1 Electrophoretic SCODA

Electrophoretic SCODA transport was performed by preparing an agarose gel in a custom square gel boat, preparing and inserting four separate spots of DNA into the gel, and then applying the appropriate potentials to four electrodes built into the four sides of the gel boat, to produce an approximation of uniform and quadrupole electric field patterns (see Fig. 2). The gel consisted of 8–11 mL 0.25% agarose gel (Agarose 2125, OmniPur, EMD Chemicals, Gibbstown, NJ, USA) in 0.1 X Tris-acetate-EDTA (TAE) buffer. DNA was visualized by adding ethidium bromide (12 μ L at 500 μ g/mL) to the gel and imaging it under UV light. The gel boat forms a 3.8 cm square over a UV transparent acrylic base. Four gold electrodes extend across one-third of each side of the gel boat, approximately 2.5 mm from the bottom of the gel boat. The electrodes are submerged in the gel. DNA was prepared by mixing 8 μ L of 500 μ g/mL λ phage DNA (48 502 bp, part No. N3011L; New England Biolabs, Beverly, MA, USA) with 12 μ L 0.1 X TAE. The DNA was pipetted directly into the gel once the gel was set, and arrayed as

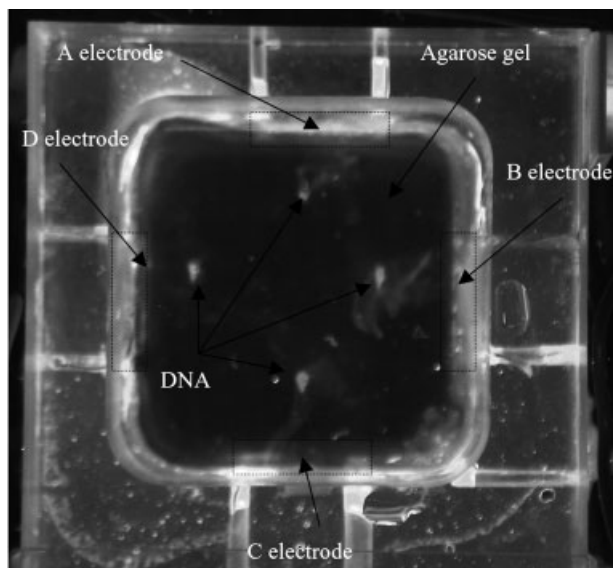


Figure 2. Photograph (under UV illumination) of the gel apparatus used for electrophoretic SCODA, including four DNA spots prior to SCODA transport.

a diamond of four spots each approximately the same distance (0.5–1.5 cm) from the estimated center of the electrode pattern. Each of the four spots consisted of 5 μ L of the above mixture. A thin covering of 0.1 X TAE was placed on the gel after the DNA was inserted and the covering was maintained over the run. The electrodes are connected to Kepco (Flushing, NY, USA) BOP 200–1M amplifiers that are in turn controlled by LabVIEW (National Instruments, Austin, TX, USA) software and a data acquisition card (NI PCI-6711; National Instruments). To simulate the electric fields described by Eqs. (11), (12), (15), and (16), without requiring analog control of the applied potentials, sinusoidal voltages were approximated by discrete forms as shown in Fig. 3. Each period of the sinusoid is represented by 12 discrete voltages, leading to 12 distinct sets of potentials applied to the electrodes during SCODA electrophoresis.

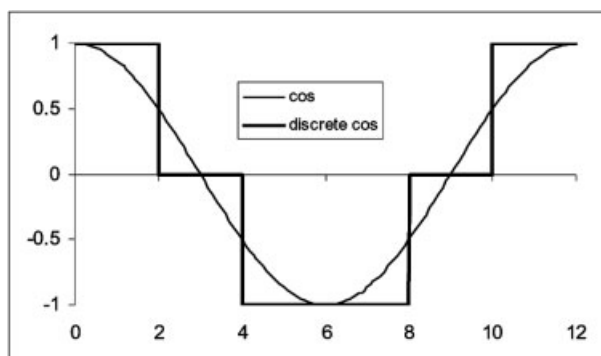


Figure 3. Discrete approximation of sinusoidal applied potentials.

Table 1. Normalized discrete potentials applied to each electrode to simulate continuous SCODA potentials

Time interval	A electrode			B electrode			C electrode			D electrode			Totals		
	au	aq	at	bu	bq	bt	cu	cq	ct	du	dq	dt	ux	uy	uq
1	0	1	1	1	-1	0	0	1	1	-1	-1	-2	2	0	4
2	1	0	1	1	0	1	-1	0	-1	-1	0	-1	2	2	0
3	1	-1	0	0	1	1	-1	-1	-2	0	1	1	0	2	-4
4	1	-1	0	0	1	1	-1	-1	-2	0	1	1	0	2	-4
5	1	0	1	-1	0	-1	-1	0	-1	1	0	1	-2	2	0
6	0	1	1	-1	-1	-2	0	1	1	1	-1	0	-2	0	4
7	0	1	1	-1	-1	-2	0	1	1	1	-1	0	-2	0	4
8	-1	0	-1	-1	0	-1	1	0	1	1	0	1	-2	-2	0
9	-1	-1	-2	0	1	1	1	-1	0	0	1	1	0	-2	-4
10	-1	-1	-2	0	1	1	1	-1	0	0	1	1	0	-2	-4
11	-1	0	-1	1	0	1	1	0	1	-1	0	-1	2	-2	0
12	0	1	1	1	-1	0	0	1	1	-1	-1	-2	2	0	4

The quadrupole component of the field is formed by applying equal potentials to opposing electrodes, and opposite potentials to adjacent electrodes. Table 1 lists the relative potentials at each of the four electrodes of Fig. 2, given discrete approximations of the uniform field from Eqs. (11) and (12) and the quadrupole field from Eqs. (15) and (16). Note that the oscillation frequency of the quadrupole field is twice that of the uniform field as required. As in Fig. 2, electrodes B-D lie in the *x*-direction, and A-C lie in the *y*-direction. Uniform field components are denoted by the suffix “u”, while the quadrupole field components are denoted by “q”. Figure 4 shows a finite element calculation (COSMOS, Structural Research and Analysis Corp., Los Angeles, CA, USA) of the (a) quadrupole field and (b) uniform field that are rotated and superposed to generate the SCODA field configuration. To simplify the electronics, one of the electrodes, arbitrarily picked to be electrode C, is set to zero potential for all time intervals, and the other electrode potentials are shifted accordingly. Performing this transformation and scaling the potentials by the actual applied voltage leads to the final form of the applied potentials listed in Table 2. Each pattern of potentials was applied to the electrodes for one second, thus cycling through all patterns every 12 s.

2.2 Numerical simulation of particle motion

A numerical simulation of particle motion under the SCODA potential pattern of Table 2 was performed using LabVIEW. A 2-D solution for the potentials in the plane of the gel was found for each electrode pattern by using a finite difference method in Matlab 6.5.1 (The Mathworks, Natick, MA, USA). Potentials were found on a 60 × 60

Table 2. Potential patterns applied to the electrodes of Fig. 2 to generate SCODA electrophoretic transport

Pattern	A Electrode	B Electrode	C Electrode	D Electrode
1	0 V	-66 V	0 V	-198 V
2	132 V	132 V	0 V	0 V
3, 4	132 V	198 V	0 V	198 V
5	132 V	0 V	0 V	132 V
6, 7	0 V	-198 V	0 V	-66 V
8	-132 V	-132 V	0 V	0 V
9, 10	-132 V	66 V	0 V	66 V
11	-132 V	0 V	0 V	-132 V
12	0 V	-66 V	0 V	-198 V

Electrode C was arbitrarily chosen as the ground electrode.

matrix representing the gel, with appropriate boundary conditions for the edges of the gel exposed to the electrodes. The LabVIEW code performs a simulation of particle motion based on an empirical function for the particle mobility, and the dependence of this mobility on electric field. The electric field at the position of each particle in the simulation is arrived at by finding the gradient of a fourth order polynomial fit to the potential in the neighbourhood of the particle. The particle motion for the next time step is then calculated as:

$$\Delta \vec{r} = \mu(E) \vec{E} \Delta t \text{ where } \mu(E) = \mu_0 + kE \quad (20)$$

Parameters for the simulation were set to the measured values $\mu_0 = 1.4 \times 10^{-9} \text{ m}^2/\text{Vs}$, $k = 2.5 \times 10^{-12} \text{ m}^3/\text{V}^2\text{s}$, with $\Delta t = 100 \text{ ms}$, and the potentials as described in Table 2.

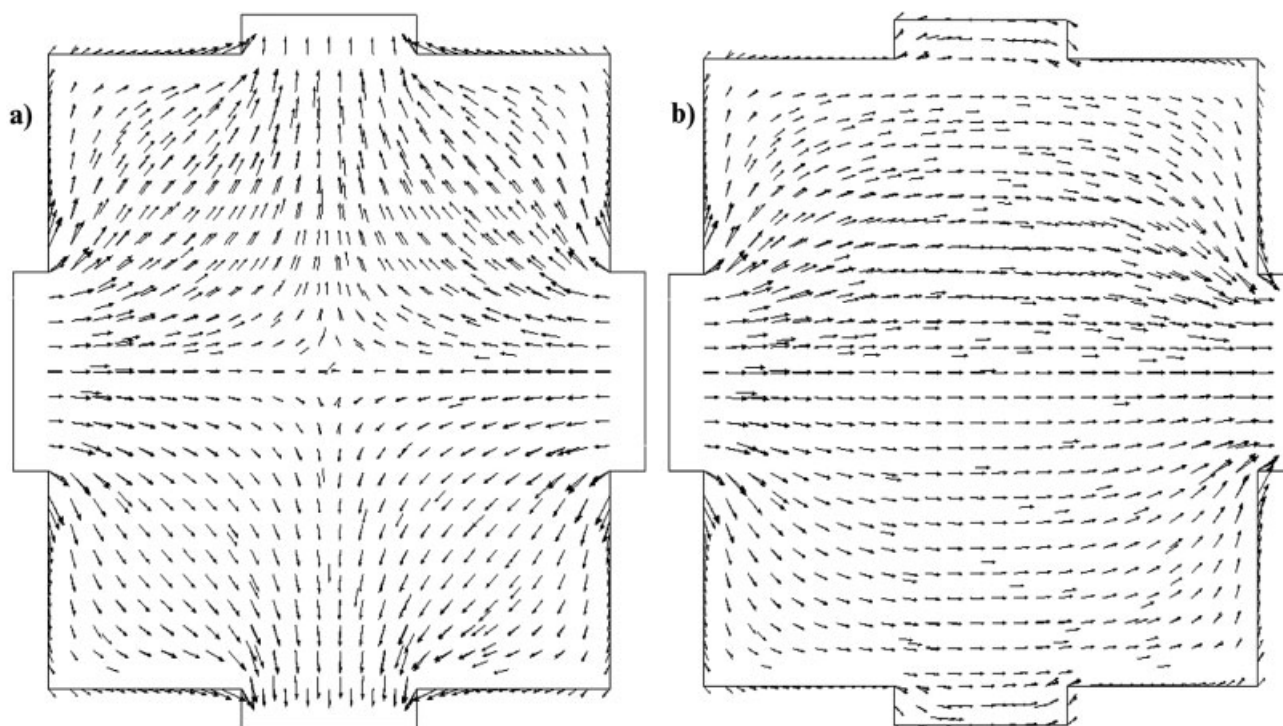


Figure 4. Electric fields present in the gel during SCODA as calculated by finite element analysis. Field direction is represented by arrows; field amplitude is approximated by the arrow length and color (not shown). Electrode locations are shown as rectangular ports in the side of the gel. The quadrupole field (a) has a point of zero amplitude in the center of the gel, while the uniform field (b) is approximately constant in amplitude and direction in this region. The quadrupole field and uniform field are rotated in the plane of the gel and superposed to obtain the resultant SCODA time-dependent field configurations. The quadrupole field rotates at twice the angular frequency of the uniform field.

2.3 Mobility measurements

To make appropriate λ phage DNA mobility measurements, the same gel concentration and electrode separation were used as in the regular SCODA experiments, except a larger gel boat (C.B.S. Scientific, CBMGU-202T, Del Mar, CA, USA) was used for ease of measurement. The same computer/amplifier connection was also used. Two gold electrodes were glued to the bottom of the gel boat across its width at a separation of 3.8 cm. A gel of the same thickness and concentration was poured and two 5 μ L samples of λ phage DNA were inserted \sim 2 mm from the ground electrode. The other electrode was connected to a Kepco BOP 200–1M power supply. A custom LabVIEW program was written that raised the voltage of the connected electrode by 25V in 2 min intervals (0–200 V). The timer on the camera was synchronized to take a picture after every voltage increase. The DNA velocity was obtained from successive images, and plotted against the electric field to obtain mobility.

3 Results and discussion

An electrophoretic demonstration of SCODA transport and focusing was performed using the equipment and methods described in Section 2.1. DNA was chosen for this experiment partly because of the well-known non-linear dependence of its drift velocity on electric field [7–9, 15, 16]. Figure 5 illustrates transport of four DNA spots toward the center of the electrode pattern, resulting in transport of all four spots into a single concentrated central spot. The motion of a particle in the experimental test of SCODA can be estimated by analyzing the motion of the intensity centroids of the four DNA spots in Fig. 5 and other similar experiments. This estimate relies on the approximation that the SCODA effect is approximately constant over the spot area – though this is not strictly correct, we found that, after the initial motion, spots change very little in morphology and size prior to merging with other spots, and therefore it appears that the entire spot can be reasonably treated as a single particle.

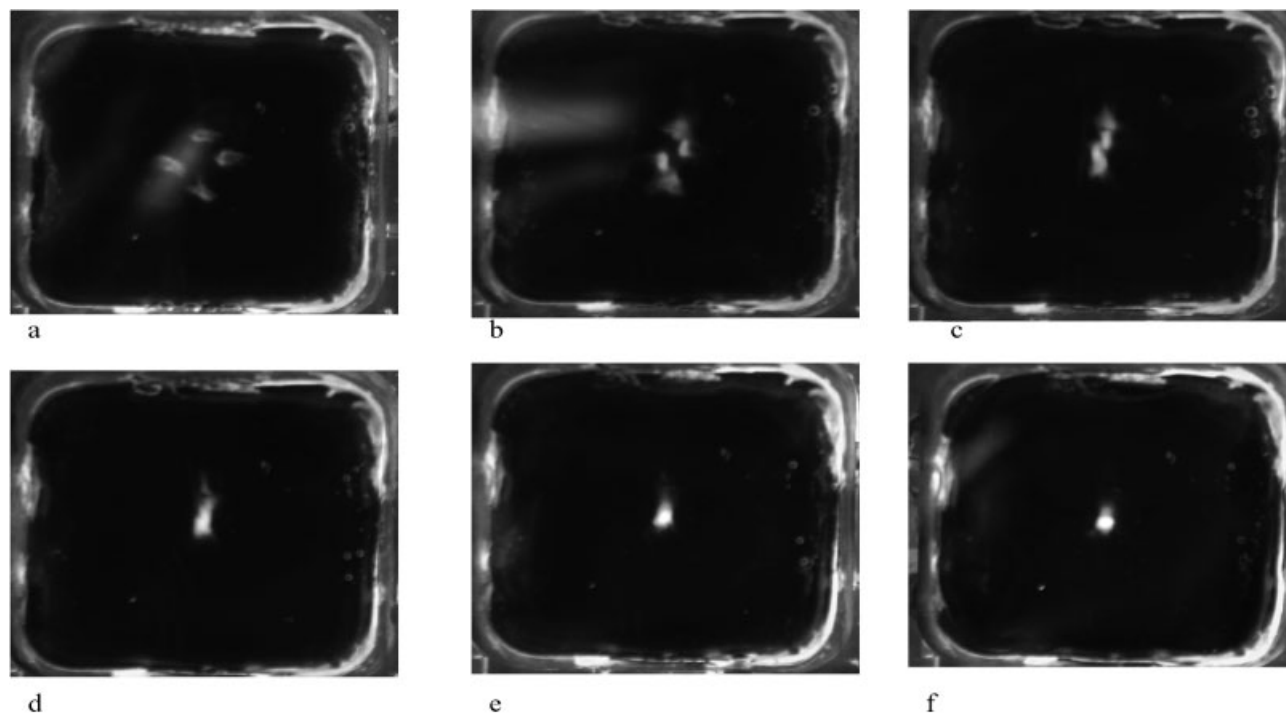


Figure 5. Electrophoretic transport of four DNA spots in an agarose gel using the SCODA effect. All spots move toward the center of the electrode pattern, though the top and bottom spots initially move more slowly, possibly due to inhomogeneity in the gel. Snapshots were taken with a digital camera under UV illumination. The elapsed time between successive images is 20 min, and the initial spot separation is approximately 1 cm.

To compare the experimental results with predictions from the analytic and numerical models, the constant and linear mobility terms need to be measured independently of the SCODA experiments. Figure 6 is a plot of measured DNA velocity as a function of electric field strength for the DNA and conditions used in the SCODA experiments. The measured DNA velocity has components both linear and quadratic with the applied electric field. The mobility therefore takes the form:

$$\mu(E) = \mu_0 + kE \quad (21)$$

where μ_0 is $1.4 \times 10^{-9} \text{ m}^2/\text{Vs}$ while the field-dependent term of Eq. (4) is $k = 2.5 \times 10^{-12} \text{ m}^3/\text{V}^2\text{s}$.

The field independent mobility μ_0 will not contribute to the SCODA effect, so the effective mobility for our purposes can be estimated as per Eq. (4) with the above value of k . This is the only parameter (other than fixed geometric and voltage parameters) required for a direct prediction of the SCODA effect from the numerical model. The analytic model of Eq. (19) requires in addition an estimate of the uniform and quadrupole field strengths at the center (origin) of the electrode pattern. These estimates are derived from Matlab finite difference solutions in the plane of the gel given the boundary potentials listed in Table 2: $E = 3845 \text{ V/m}$, $E_q = 4.2 \times 10^5 \text{ rV/m}$.

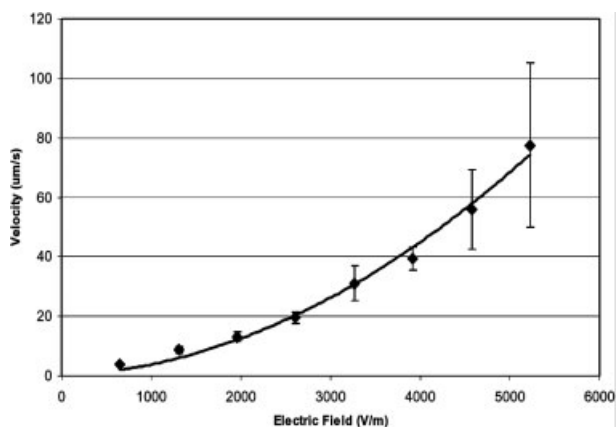


Figure 6. Measured velocity of λ phage DNA (48.5 kbp) as a function of electric field. See Section 2 for conditions. The solid line is a quadratic polynomial fit to the data and takes the form: $v = 1.4 \times 10^{-9} \frac{\text{m}^2}{\text{Vs}} E + 2.5 \times 10^{-12} \frac{\text{m}^3}{\text{V}^2\text{s}} E^2$

Figure 7 shows a comparison of measured DNA spot distance from the origin as a function of time, compared to numerical and analytic predictions. The spot position is averaged over all spots visible in a given time interval. Spot trajectories for spots starting at different radial dis-

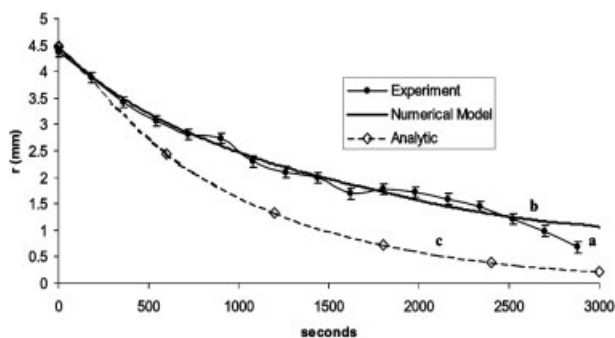


Figure 7. Averaged radial distance of DNA spots from the origin plotted from (a) experimental results, (b) numerical predictions, and (c) analytic prediction (Eq. 19). Error bars denote uncertainty in the determination of the spot centroids.

tances from the origin are shifted in time such that the start time for trajectories starting closer to the origin is replaced by the time at which the other trajectories reach the starting distance.

Agreement between the model and experiment is good in the regime shown in Fig. 7. The analytic prediction, on the other hand, relies on a small-signal analysis of the quadrupole field and is therefore not expected to exactly predict the experimental trajectories in this case where the quadrupole field is of comparable amplitude to the uniform field. Nevertheless, it is encouraging that the form of the behavior is substantially the same in this simple analytic model.

Figure 8 is a plot of average spot velocity (time averaged over 15 min) as a function of radial distance from the origin, showing explicitly the linear dependence of velocity on distance expected from the analytic model. Two curves are shown for the numerical model – one for a particle trajectory started in the x -axis, and one for a particle started at $x = y = 1.5$ cm from the origin. The difference in the two curves as the distance from the origin increases reflects the azimuthal asymmetry in the time-averaged electric field pattern that results from the finite size of the electrodes. The numerical model and experiment agree well only for short distances to the origin, beyond which the experimentally measured velocity becomes nearly independent of distance. It is expected that at larger distance from the origin, particles experience fields greater than those explored in our mobility measurements. Since the numerical model is based on the mobility measurements, it is only valid for the range of electric field amplitudes explored in the measurements of Fig. 6. Effects resulting from larger field amplitudes are not accounted for and may be responsible for the observed deviation from the model.

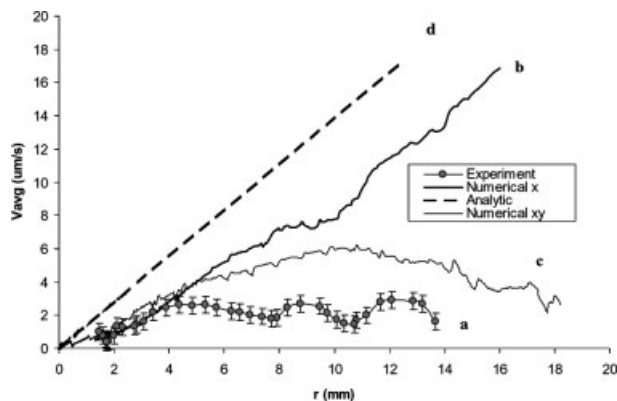


Figure 8. Average DNA velocity as a function of radial distance of DNA spots from the origin plotted from (a) experimental results, (b) numerical simulation (started at $x = 1.5$ cm, $y = 0$), (c) numerical simulation (started at $x = 1.5$ cm, $y = 1.5$ cm), and (d) analytic prediction of Eq. (19). Experimental data below $r = 1$ mm is not available due to difficulty in extracting individual spot centroids once the spots begin overlapping at the center of the image. The error bars are based on uncertainty in the determination of the spot centroids.

Although we attempted to place the DNA spots in the experiment along the x - and y -axes defined by the electrodes, placement of the spots may not have been exactly on axis and this may be reflected in part in the spot trajectories. Occasionally (as seen in Fig. 5) spot velocities did not follow the expected symmetry – this is suspected to result from nonhomogeneity in the agarose gel, as it did not occur in every experiment nor did this always affect the same spots.

Though this work is intended primarily to demonstrate SCODA transport of DNA, it is clear that DNA, and possibly other charged polymers, can be spatially concentrated using SCODA. The limiting radius of the concentrated spot shown in Fig. 5 can be estimated from the Einstein-Smoluchowsky equation for diffusion with drift:

$$\frac{\partial C}{\partial t} = D \nabla^2 C + \mu \nabla \cdot (\vec{E} C) \quad (22)$$

Using Eq. (19) to replace the electrophoretic drift term with SCODA drift, and rewriting in cylindrical coordinates we have:

$$\frac{\partial C}{\partial t} = D \frac{1}{r} \frac{\partial}{\partial r} \left(r \frac{\partial C}{\partial r} \right) + \mu_s \frac{1}{r} \frac{\partial}{\partial r} (r^2 C) \quad (23)$$

where $C(r, t)$ is the DNA concentration, D is the diffusion coefficient, and

$$\mu_s = \frac{k E E_q}{4} \text{ is a SCODA "mobility" from Eq. (19).}$$

Dimensional inspection of Eq. (23) yields a characteristic length scale for the radius of the focused spot to be

$$R \propto \sqrt{\frac{D}{\mu_s}} \quad (24)$$

Using the experimentally measured D (2×10^{-12} m²/s) and deriving μ_s from the slope of the model and experiment data near $r = 0$ (Fig. 8) ($\mu_s \sim 1 \times 10^{-3}$ 1/s) we get an estimate for the limiting spot radius to be ~ 50 μm . A numerical solution to Eq. (23) based on the same parameters yields a spot FWHM of ~ 100 μm , assuming that no DNA leaks out of the focused spot in the z -direction (orthogonal to the gel), and that the spot is saturated with DNA. Observations of spot radius (full width at half maximum (FWHM)/2) from the experiments yields limiting radii on the order of ~ 500 μm ; continued focusing leads to a decrease in fluorescent intensity, likely through diffusion of DNA in the z -direction into the buffer above the gel. It is conceivable that in conditions where such diffusion was inhibited, smaller spot sizes and higher concentrations could be achieved.

4 Concluding remarks

We have demonstrated a general method for transport of molecules in solution by application of a zero-time-averaged force, and a synchronous perturbation of the mobility or drag of the molecule by thermal or electrophoretic means. Optical or other forms of this method should also be feasible but remain to be demonstrated. The SCODA method offers the advantage of being able to concentrate molecules in regions defined by the perturbing mechanism. In the electrophoretic case, we have demonstrated the ability to transport DNA distributed in a gel to a region in the centre of the gel that is free of electrodes. This method is likely to have impact on DNA purification, extraction, and concentration.

The authors wish to thank Robin Coope, Elliot Holtham, and David Broemeling for helpful discussions and assistance with this work. This work is funded in part by the National Human Genome Research Institute of NIH, under grant HG002743.

5 References

- [1] Ferapontova, E. E., Shipovskov, S. V., *Biochemistry (Moscow, Russ. Fed.)* 2003, 68, 99–104.
- [2] Dryhurst, G., *Electrochemistry of Biological Molecules*, Academic Press, New York 1977.
- [3] Sambrook, J., Fritsch, E. F., Maniatis, T. (Eds.), *Molecular Cloning: A Laboratory Manual*, Cold Spring Harbor Laboratory Press, Cold Spring Harbor, New York 1989.
- [4] Meldrum, D., *Genome Res.* 2000, 10, 1288–1303.
- [5] Wilson, I. D., Adlard, E. R., Cooke, M., Poole, C. F. (Eds.), *Encyclopedia of Separation Science*, Academic Press, San Diego, CA 2000.
- [6] Cheng, J., Sheldon, E. L., Wu, L., Uribe, A., Gerrue, L. O., Carrino, J., Heller, M. J., O'Connell, J. P., *Nat. Biotechnol.* 1998, 16, 541–546.
- [7] Slater, G. W., Desruisseaux, C., Hubert, S. J., Mercier, J. F., Labrie, J., Boileau, J., Tessier, F., Pepin, M. P., *Electrophoresis* 2000, 21, 3873–3887.
- [8] Lumpkin, O. J., Dejardin, P., Zimm, B. H., *Biopolymers* 1985, 24, 1573–1593.
- [9] McDonnell, M. W., Simon, M. N., Studier, F. W., *J. Mol. Biol.* 1977, 110, 119–146.
- [10] Slater, G. W., Kist, T. B. L., Ren, H., Drouin, G., *Electrophoresis* 1998, 19, 1525–1541.
- [11] Tessier, F., Slater, G. W., *Appl. Phys. A* 2002, 75, 285–291.
- [12] Slater, G. W., Guo, H. L., Nixon, G. I., *Phys. Rev. Lett.* 1997, 78, 1170–1173.
- [13] Griess, G. A., Rogers, E., Serwer, P., *Electrophoresis* 2000, 21, 859–864.
- [14] Griess, G. A., Choi, H., Basu, A., Valvano, J. W., Serwer, P., *Electrophoresis* 2002, 23, 2610–2617.
- [15] Chacron, M. J., Slater, G. W., *Phys. Rev. E* 1997, 56, 3446–3450.
- [16] Frumin, L. L., Peltek, S. E., Bukshpan, S., Chasovskikh, V. V., Zilberstein, G. V., *Phys. Chem. Commun.* 2000, 11.
- [17] Frumin, L. L., Peltek, S. E., Zilberstein, G. V., *Phys. Rev. E* 2001, 64, 021902.
- [18] Pohl, H.-A., *Dielectrophoresis: The Behavior of Neutral Matter in Nonuniform Electric Fields*, Cambridge University Press, Cambridge, UK 1978.
- [19] Asbury, C. L., Diercks, A. H., van den Engh, G., *Electrophoresis* 2002, 23, 2658–2666.
- [20] Asbury, C. L., van den Engh, G., *Biophys. J.* 1998, 74, 1024–1030.
- [21] Dürr, H., Bouas-Laurent, H. (Eds.), *Photochromism: Molecules and Systems*, Elsevier, New York, NY 1990.
- [22] Liang, X., Asanuma, H., Komiyama, M., *J. Am. Chem. Soc.* 2002, 124, 1877–1883.
- [23] Rosario, R., Gust, D., Hayes, M., Jahnke, F., Springer, J., Garcia, A. A., *Langmuir* 2002, 18, 8062–8069.